XL CILAMCE
IBERO-LATIN AMERICAN CONGRESS ON COMPUTATIONAL METHODS IN ENGINEERING
NOVEMBER 11-14, 2019
Praiamar Natal Hotel & Convention Natal, RN-BRAZIL

EVALUATION OF THE BEHAVIOR OF MONOPILE FIXED OFFSHORE WIND TURBINES

Gabriel Nogueira
Gilberto B. Ellwanger
José R. M. de Sousa
gabriel.nogueira@laceo.coppe.ufrj.br
gbe@laceo.coppe.ufrj.br
jrenato@laceo.coppe.ufrj.br
Department of Civil Engineering, Federal University of Rio de Janeiro
Av. Athos da Silveira Ramos, 149, 21941-909, Ilha do Fundão, Rio de Janeiro, Brazil

Abstract. This work follows a worldwide trend of developing new wind farm projects on sea. Standard models used by the academy of 5 and 10 MW wind turbines are introduced to the Brazilian environment being supported by fixed foundations of the monopile type. The aim is to develop a sensitivity analysis of the fatigue damage in a critical point of the foundation under the effect of important offshore cyclic loads. The models employed in this paper were firstly validated through analyses of their natural frequencies. The next step was to subject them to extreme loads caused by wind, wave and current to determine the critical point in each turbine's foundation. With these points in hand, the sensitivity analysis was conducted assuming the wind with and without a dynamic component, while the sea waves were represented by the Jonswap or Pierson-Moskowitz spectrum. Finally, fatigue was assessed through the damage calculated by the Palmgren-Miner rule in association with the largely employed S-N curves and the rainflow method for counting stress cycles in the time series generated by SIMA-RIFLEX. This study showed the importance of the dynamic component of the wind in the structure's lifespan, which was reduced by at least one order of magnitude when considered. No significant change in fatigue damage was observed with different wave spectra. Lastly, life results obtained for the 10 MW turbine were better than the 5 MW due to its more robust geometric characteristics.

Keywords: Wind turbine, Offshore structures, Fatigue, Sensitivity analysis

1 Introduction

According to the Brazilian Energy Review of 2018 [1], 80.4% of the domestic supply of electricity comes from renewable sources. An excellent indicator compared to the world average of only 24.9%. As shown by the energy review, 81.2% of this renewable supply comes from hydroelectric power plants.

In the Brazilian context, the supremacy of hydroelectric power is characterized by its inconsistency in supplying the country's energy needs. The population often faces headlines highlighting the low levels of water in the reservoirs and the government's expensive exit for this problem in the thermoelectric power plants. In addition to this scenario is the high waste of electric energy. In Brazil, this rate reaches 16% (Brazilian Energy Review [1]), which is well above the value observed in other countries. This high index is the result of both the technical losses (amount of energy dissipated between the supply and the point of delivery) and the clandestine connections.

On the other hand, in order to reduce the impact of the drought that has affected the Northeastern region of Brazil for more than six years, causing serious problems in the production of energy by the São Francisco Basin's hydroelectric power plants, the wind power source emerged as the main solution and already accounts for more than 50% of the region's energy. According to the Brazilian Energy Review [1], wind energy is one of the sources that most thrived between 2016 and 2017 (26.5%).

The country already has considerable experience with onshore wind farms that produced, in 2017, 42.4 TWh (Brazilian Energy Review [1]). However, the novel projects worldwide are being designed to the offshore environment. Brazil, however, does not have any offshore wind farm in operation yet. This trend started for a number of reasons, such as better wind conditions at sea, closer proximity between the wind farms and the large consumer centers (big cities and industries) and consequent reduction of transmission lines, as well as reduction of the visual-sound impact caused by these structures. Another important factor for this trend is the increase in size of the wind turbines (in particular turbines larger than 7.5 MW). This made difficult to install them on land because of logistical problems such as transportation of the turbine's components.

Therefore, the motivation for this work was not only due to its environmental or strategic importance for the nation, but mainly for the offshore wind potential not yet explored in the Brazilian territory. It is unlikely that the dominant hydroelectric power will be replaced by the rising wind energy in Brazil. However, it is possible for wind power to respond at critical periods of the system and make non-renewable energies a more distant option.

In order to start understanding the behavior of fixed offshore wind turbines, the main objective of this work is to study the fatigue damage variation at a critical point in their foundation. Two turbine models were used: a 5 MW turbine, developed by Jonkman *et al* [2] at NREL (National Renewable Energy Laboratory), and another one of 10 MW, made by Bak *et al* [3] at DTU (Technical University of Denmark), each supported by its own monopile. With these models in hand, it is expected to determine, under Brazilian environmental conditions, how much the fatigue damage varies when modeling the sea waves through the Jonswap or Pierson-Moskowitz spectrum and the wind with and without its dynamic component.

After validating the models created in SIMA-RIFLEX software [4] through a study of the natural frequencies, a preliminary analysis, where extreme wave, current and wind acts, is performed in order to determine the critical point of the foundation of each turbine. With these points in hand, the selection of the loading cases acting on the turbines is made based on the surveyed data of the Brazilian coast and on current norms/methodologies in the literature. Finally, fatigue is computed using the Palmgren-Miner rule in association with the S-N curves presented by DNV-RP-C203 [5] and with the rainflow method for counting the stress cycles at the critical point of the foundation.

2 Wind Turbine Modeling

2.1 Turbine and foundation dimensions

Figure 1 shows the four models that were elaborated in SIMA-RIFLEX [4]. Models 1 and 2 consider the 5 and 10 MW wind turbines, respectively, with their tower fixed onshore (without the foundation). These two are the standard academic models developed by Jonkman *et al* [2] and Bak *et al* [3] and served as the basis for a series of other projects that aimed to couple them on various types of foundations, such as the OC3 project (Jonkman and Musial [6]). Models 3 and 4 are effectively the first two models with modifications in tower geometry and supported by a monopile foundation. Both are in an offshore environment with a 20 meters mean-sea level. Their characteristics were obtained from Jonkman and Musial [6] and Velarde and Bachynski [7]. The fatigue studies in this paper focus on the last two models.

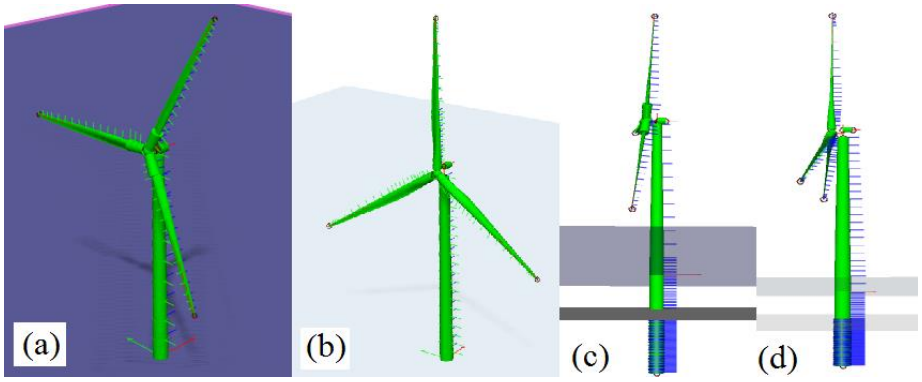

Figure 1. Models elaborated in SIMA-RIFLEX [4]: (a) Model 1: 5 MW onshore; (b) Model 2: 10 MW onshore; (c) Model 3: 5 MW offshore; (d) Model 4: 10 MW offshore (Nogueira [8]).

In Jonkman *et al* [2] and Bak *et al* [3], there is plenty of information about the towers geometries, control systems, nacelles characteristics and geometric and aerodynamic data of the rotors (including the types of airfoils used, which is hardly provided by the industry). In addition, these documents provide the natural frequencies of the onshore wind turbines (models 1 and 2) and a series of charts and tables containing the values of the aerodynamic loads (thrust, torque, power, etc.) that aided in the calibration of the models presented in this work. Table 1 shows the mechanical properties of the steel used in the towers body and monopile foundations (models 3 and 4). The mass density of 8500 kg/m³ was assumed to consider the presence of secondary structures. Table 2 summarizes the main information of models 1 and 2. Both wind turbines actively control the pitch angles of their blades for maximum wind power and operational safety of the structure.

Table 3 summarizes the data that has been modified or added to adjust from model 1 to model 3 and from model 2 to model 4. It is interesting to note how the consideration of the transition piece (a component of the turbine that connects the tower to the foundation) was made in these models: In Jonkman and Musial [6], this component was completely neglected (model 3), while in Velarde and Bachynski [7], this piece was modeled as a concentrated mass at a 19 meters elevation above the mean-sea level (model 4). The rotors, the control systems and the nacelles remain identical during the models' adjustment.

Table 1. Steel's mechanical properties.

Young's modulus	210 GPa
Shear modulus	80.8 GPa
Mass density	8500 kg/m³

Table 2. 5 and 10 MW onshore wind turbines' properties (Jonkman *et al* [2]; Bak *et al* [3]).

Properties	5 MW	10 MW
Tower length (m)	87.6	115.63
Rotor diameter (m)	126	178.3
Hub height (m)	90	119
Hub diameter (m)	3	5.6
Tilt angle (º)	5	5
Precone angle (º)	2.5	2.5
Overhang (m)	5	7.1
Tower external diameters (top/base) (m)	3.87; 6	5.5; 8.3
Tower thickness (top/base) (mm)	24.7; 35.1	20; 38
Number of blades	3	3
Rotor orientation	upwind	upwind
Cut-in, cut-out and nominal wind speed (m/s)	3; 25; 11.4	4; 25; 11.4
Cut-in, rated rotor speed (rpm)	6.9; 12.1	6; 9.6

Table 3. 5 and 10 MW offshore wind turbines' properties (Jonkman and Musial [6]; Velarde and Bachynski [7]).

Properties	5 MW	10 MW
Mean-sea level (m)	20	20
Tower length (m)	77.6	115.63
Transition piece mass (kg)	--	500000
Transition piece position above sea level (m)	--	19
Tower external diameters (top/base) (m)	3.87; 6	6.25; 9.5
Tower thickness (top/base) (mm)	19; 27	25; 47.5
Monopile diameter (m)	6	9
Monopile thickness (mm)	60	110
Monopile length (m)	36 (below mudline) 30 (above mudline)	35 (below mudline) 20 (above mudline)

2.2 Soil-foundation interaction

In order to model the soil-foundation interaction, a common practice in the wind energy industry is the adoption of decoupled translational springs. In this work, only the lateral resistance of the soil was considered and, to represent it, non-linear p-y springs were used, which are defined in API-RP2A-WSD [9]. In SIMA-RIFLEX [4], this methodology was possible to be employed due to the software feature of defining springs through a graph of Lateral Strength (N) vs Displacement (m). The springs' stiffness varies according to depth as they were discretized for each meter of soil layer (Fig. 2).

The monopiles of models 3 and 4 are interacting with the same uniform layer of typical sand of the Brazilian coast. The monopiles are filled with sand below the mudline. Above it and up to the mean-sea level, the monopiles are filled with sea water. The soil data for the composition of the p-y curves are presented in Table 4.

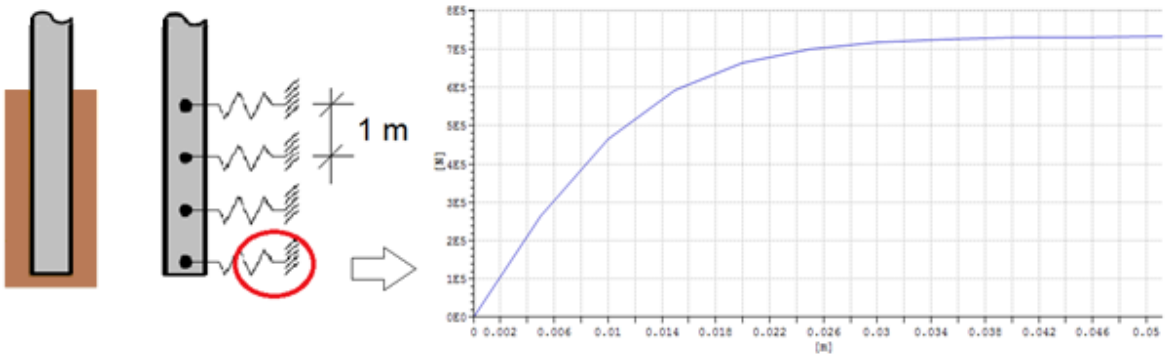

Figure 2. Representation of soil-foundation interaction through the adoption of non-linear translational springs in SIMA-RIFLEX (adapted from Nogueira [8]).

Table 4. Soil data (Nogueira [8]).

Angle of internal friction of the sand (º)	35
Initial modulus of subgrade reaction (kN/m³)	22000
Effective soil weight (kN/m³)	8.5

2.3 Aerodynamic loads

The real wind velocity is represented by a static and a dynamic component. To represent the mean wind speed (static part), the power-law profile was used in this paper with a 0.14 exponent typical of offshore environments (DNV-OS-J101 [10]), as written in Eq. (1):

$$U_m(z) = U_m(z_{ref})\left(\frac{z}{z_{ref}}\right)^{0.14}, \tag{1}$$

where U_m(z) is the mean wind speed at a height 'z' above mean-sea level and $U_m(z_{ref})$ is the mean wind speed at reference height z_{ref} above mean-sea level (in this paper, 10 meters).

The dynamic component, labeled turbulence of the wind, is caused by eddies that are carried along the flow at the mean wind speed. These eddies are randomly distributed in space and possess equally random periods and sizes. The best way to represent the dynamic component is through a spectral model. The one recommended by DNV-OS-J101 [10] and used in this paper is the Kaimal spectrum. Its formulation can be found in TurbSim user's guide (Jonkman and Kilcher [11]), a software capable of generating realistic wind and compatible with SIMA-RIFLEX [4]. The Kaimal spectrum formulation, as stated in the user's guide, is defined by Eq. (2):

$$S(f) = \frac{\frac{4\sigma^2 L}{U_{m,hub}}}{\left(1+\frac{6fL}{U_{m,hub}}\right)^{5/3}}, \tag{2}$$

where S is the power spectrum density function, f is the frequency, $U_{m,hub}$ is the mean wind speed at the hub height, σ is the standard deviation and L is the integral scale parameter.

To calculate the aerodynamic loads acting on the rotor, SIMA-RIFLEX [4] utilizes the Blade Element Momentum Theory (BEMT). The concept behind this theory is the compatibilization between the linear and angular momentum theories that analyze the air flow before and after its passage through the rotor and the local events that take place in the various blade elements (Fig. 3). This is very important since the momentum theories disregard the blade's geometry.

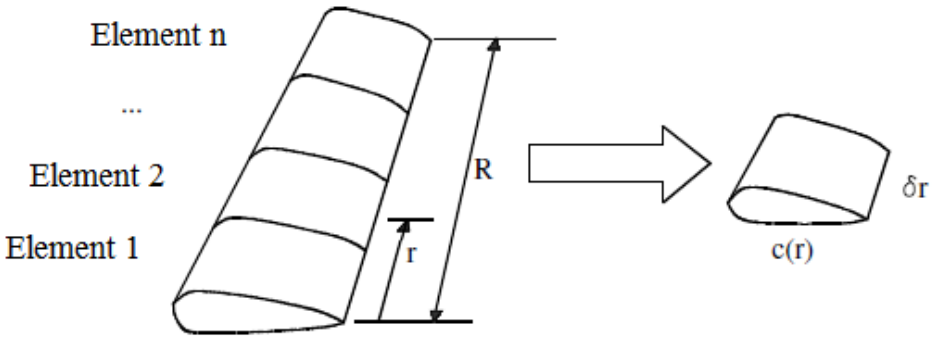

Figure 3. Blade discretization into 'N' elements (adapted from Maiolino [12]).

The complete description of BEMT and its necessary corrections can be found in Hansen [13]. There, an algorithm is proposed to find the axial and tangential induction factors and, ultimately, the thrust force and the torque on the rotor.

2.4 Hydrodynamic loads

An offshore wind turbine is also under the effect of forces caused by waves and currents. In this work, the sea current is assumed to be a static load. The loads produced by it were calculated through the Morison formulation (Morison *et al* [14]), which is widely employed in practical applications for the assessment of fluid forces in slender bodies.

Like the wind, the sea waves present a random behavior and are better described by spectral models. In the sensitivity analysis, two options were adopted with SIMA-RIFLEX [4]: the Jonswap and the Pierson-Moskowitz spectrums, both typically used on the Brazilian coast.

However, a centenary regular wave was chosen to define the critical point in order to avoid randomness in its position and to simulate an extreme condition. Two wave theories are present in the software [4]: Airy's linear theory and Stokes' 5th order theory. Depending on the wave height *H*, the wave period *T* and the water depth *d* in which the wave propagates, the theory that best represents reality may change. The API-RP2A-WSD [9] presents a graph in which regions of applicability for different wave theories are defined. These theories describe the kinematics of fluid particles at any position of the wave in distinct ways (accelerations, velocities, particle elevation). These magnitudes ultimately affect the evaluation of the hydrodynamic forces (which were also done using Morison formulation).

Since this work's purpose is to calculate the fatigue in the foundation of two distinct wind turbines using equal environmental conditions and varying only the wave spectra and the presence of the dynamic wind component, API-RP2A-WSD recommendations [9], as far as wave theories were concerned, were disregarded for simplification. More information on all these theories can be obtained in the works of Sarpkaya and Isaacson [15] and Chakrabarti [16].

2.5 Fatigue damage assessment

Fatigue damage is caused by cyclic loads. Within the scope of an offshore wind turbine foundation, the environmental loads that promote this type of damage are the wind and the sea waves. Their presence will result in the appearance of efforts that, in turn, will produce stresses. Stress variation ($\Delta\sigma$) is the cause of damage in a structure that, eventually, will fail due to fatigue. In this work, only stresses due to bending moments were considered, which is equivalent to saying, in mathematical terms:

$$\sigma = \frac{M_z}{I_z} y + \frac{M_y}{I_y} z, \tag{3}$$

where σ is the stress at a given point in the cross-section, M_y and M_z are the bending moments in the Y and Z directions (local axis of the cross section, as in Fig. 4) and $I_y = I_z = I$ is the moment of inertia of the cross section of the monopile (which is a circular ring). Fig. 4 also shows the eight cross-sectional

points for which fatigue damage was calculated. Only the damage from points 1 to 4 are presented in the sensitivity analysis because these values are symmetrical to those in points 5 to 8.

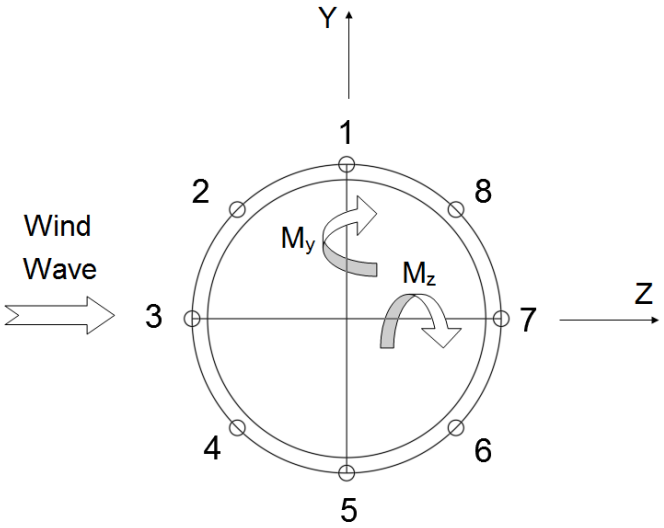

Figure 4. Points where the fatigue damage was calculated (adapted from Nogueira [8]).

After the stress time series is generated by SIMA-RIFLEX's dynamic analysis module, the software counts the stress cycles through the rainflow method, originally developed by Matsuiski and Endo [17]. According to Giraldo [18], the basic idea of the rainflow method is to identify only the peaks and valleys of the stress time series and then use a series of considerations to identify all stress cycles (and their associated $\Delta\sigma$ ranges) throughout the history of the time series.

To calculate the number of cycles to failure, SIMA-RIFLEX [4] uses the S-N curves defined in DNV-RP-C203 [5] by Eq. (4):

$$\log N = \log a - m \log\left(\Delta\sigma \left(\frac{t}{t_{ref}}\right)^{k}\right), \tag{4}$$

where a, m and k are parameters of the S-N curve, N is the number of cycles to failure at constant stress range $\Delta\sigma$, t is the thickness through which the potential fatigue crack will grow and t_{ref} is the reference thickness for which the S-N curves were generated. The fraction t/t_{ref} was assumed equal to one in this work.

With the stress cycles identified through the rainflow method and the number of cycles to failure obtained through the S-N curves, the fatigue damage is calculated by the simple sum of all the stress cycles identified by the Palmgren-Miner rule (DNV-OS-J101 [10]) given by Eq. (5):

$$Damage = \sum_{i=1}^{J} \frac{n_i}{N_i}, \tag{5}$$

where n is the number of stress cycles and J is the number of identified stress ranges $\Delta\sigma$.

In order to find the total damage on the foundation, one must multiply the value obtained in Eq. (5) by the probability of occurrence of each loading case (P) and, finally, sum:

$$Total\ Damage = \sum_{i=1}^{K} Damage_i\, P_i, \tag{6}$$

where K is the number of loading cases. The structure's lifespan is obtained by inverting Eq. (6), i.e.:

$$Lifespan = \frac{1}{Total\ Damage}. \tag{7}$$

3 Sensitivity Analysis

3.1 Model validation

To ensure that the models created are valid, a comparison of the natural frequencies of the onshore models created in SIMA-RIFLEX [4] with those provided by Jonkman *et al* [2] and Bak *et al* [3] was made. The idea behind this test was to confirm whether the number of elements adopted for the tower and the blades, for example, was sufficient to properly distribute the stiffness and mass of the turbine. Tables 5 and 6 show the results of the natural frequencies and comparisons with the appropriate sources. It can be observed that the maximum relative difference in both comparisons was below 5%, which validates both models.

Table 5. Natural frequencies comparison: 5 MW onshore wind turbine (Nogueira [8]).

Mode	RIFLEX (Hz)	NREL (Hz) [2]	Relative Difference
1	0.313	0.320	1.91%
2	0.310	0.316	1.96%
3	0.592	0.609	2.79%
4	0.629	0.630	0.05%
5	0.661	0.669	1.14%
6	0.689	0.702	1.80%
7	1.068	1.074	0.58%
8	1.081	1.088	0.66%
9	1.703	1.651	3.16%
10	1.836	1.856	1.07%

Table 6. Natural frequencies comparison: 10 MW onshore wind turbine (Nogueira [8]).

Mode	RIFLEX (Hz)	DTU (Hz) [3]	Relative Difference
1	0.24	0.25	4.00%
2	0.24	0.25	4.00%
3	0.49	0.50	2.00%
4	0.55	0.55	0%
5	0.59	0.59	0%
6	0.62	0.63	1.59%
7	0.94	0.92	2.17%
8	0.95	0.94	1.06%
9	1.41	1.38	2.17%
10	1.58	1.55	1.94%

After confirming the onshore frequencies (models 1 and 2), the following objective was to adopt the same modeling methodology for the offshore cases (models 3 and 4). The natural frequencies obtained for them are presented in Table 7. In this case, there was no direct comparison with what was described in Jonkman and Musial [6] and Velarde and Bachynski [7], since these works did not provide tables with the full system natural frequencies.

Table 7. Natural frequencies of the offshore wind turbines models (Nogueira [8]).

Mode	5 MW (Hz)	10 MW (Hz)
1	0.241	0.263
2	0.239	0.261
3	0.575	0.492
4	0.617	0.577
5	0.653	0.596
6	0.686	0.622
7	1.065	0.941
8	1.076	0.947
9	1.396	1.279
10	1.453	1.323

A significant drop in the natural frequencies of the 5 MW turbine is observed after the adjustment from model 1 to model 3. This is justified by the increase in the slenderness of the structure that occurs for two reasons: monopile's insertion in model 3 and lower tower thickness both at the base and at the top. In the adjustment of model 2 to model 4, large changes in frequencies are not noticed, as Velarde and Bachynski [7] aimed, purposely, to make the first natural frequencies of the structure close to 0.25 Hz. As the presence of the monopile would decrease the natural frequencies, the tower external diameters and thicknesses were increased to provide greater stiffness. The characteristics of the monopile as length, thickness and external diameter were also calibrated following this purpose.

Table 8 shows the number of elements that were used in each of the models, as well as the number of degrees of freedom. Spatial frame elements, which are defined by nodes that have 6 degrees of freedom (DOF) each, were adopted in all models.

Table 8. Number of elements and degrees of freedom for each model (Nogueira [8]).

Model	# Elements	# DOF
1	67	408
2	104	630
3	169	1020
4	195	1176

3.2 Critical point determination

As described in section 2.5, stress variation is what causes fatigue. The higher this variation, the greater the damage and the shorter the structure's lifespan. In order to choose a critical point in the foundation and, then, to evaluate it, it was assumed that this point would also be related to high stresses, a hypothesis also adopted by Bøhn [19].

Thus, extreme aligned wave, wind and current, typical of the Brazilian coast, were applied on models 3 and 4 according to the direction shown in Fig. 4. All values have a returning period of 100 years, except for the wind. The other considerations made in order to reach the greatest stresses possible in the foundation for this study were:

1. 11 m/s uniform wind speed profile. This value was adopted to get close to the maximum thrust without causing any changes in the pitch angle of the turbines by SIMA-RIFLEX. The hundred-year value of the wind is 19.22 m/s and would not cause the greatest possible thrust;
2. The wave was considered regular with H = 7.0 m and T = 14 s. The fifth-order Stokes theory was used to represent it, and the hydrodynamic force was calculated using the Morison formulation, since internal tests with the program showed that greater efforts would be produced with this assumption. The inertia and drag coefficients adopted were, respectively, 2.0 and 0.9;
3. 0.8 m/s uniform current profile.

As in this work only the bending moments were considered for the calculation of stress in the cross sections, the maximum stress point will also be associated with a maximum curvature.

Figure 5 show the absolute maximum stresses and the maximum total curvatures obtained along the buried section of the 5 MW's monopile (from the seabed to the foundation base at -36 meters). With the monopile discretized every 0.5 meter, it is observed that the point of maximum stress occurred 4.5 meters below the sea floor. The absolute maximum stress value was 60.566 MPa and occurred at points 3 and 7 of the cross section of Fig. 4. The maximum total curvature was $9.629.10^{-5}$ m^{-1}.

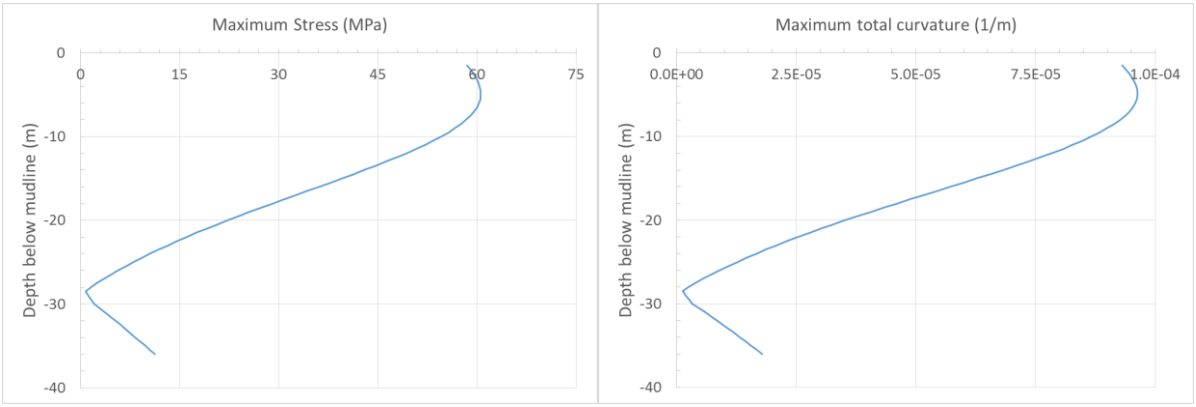

Figure 5. Maximum stresses and curvatures for the 5 MW's monopile (Nogueira [8]).

Figure 6 show the absolute maximum stresses and the maximum total curvatures obtained along the buried section of the 10 MW's monopile (from the sea floor to the foundation base at -35 meters). With the monopile discretized every 0.5 meter, it is observed that the point of maximum stress occurred 7.5 meters below the sea floor. The absolute maximum stress value was 39.911 MPa and occurred at points 3 and 7 of the cross-section of Fig. 4. The maximum total curvature was $4.226.10^{-5}$ m^{-1}.

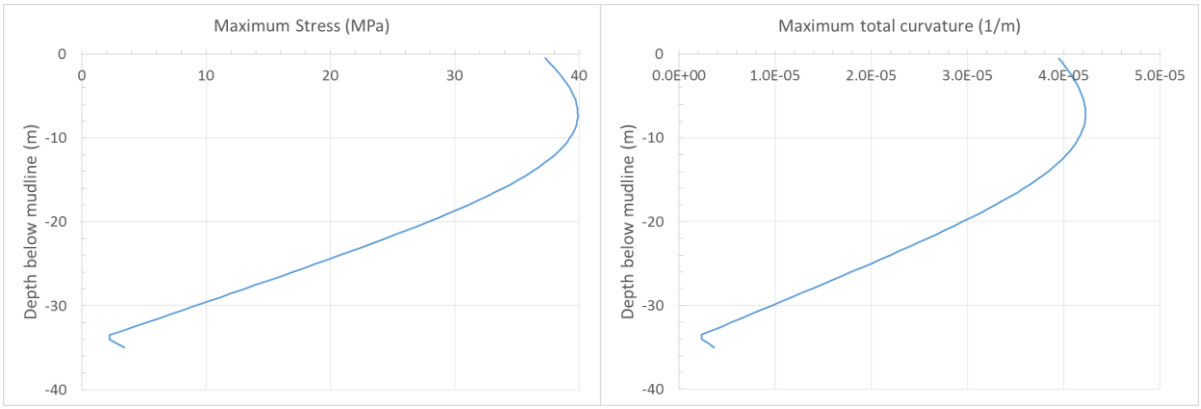

Figure 6. Maximum stresses and curvatures for the 10 MW's monopile (Nogueira [8]).

These results are very important since it is possible to note that, although the 10 MW wind turbine is under greater loads than the 5 MW (Nogueira [8]), the fact that its cross-section is more robust (providing a moment of inertia about 6 times greater) considerably reduces the stress experienced by the critical section (4.939 m^4/60.566 MPa for 5 MW turbine against 30.355 m^4/39.911 MPa for 10 MW turbine).

3.3 Loading case selection and analysis parameters

In order to obtain the total fatigue damage in an offshore wind turbine, a series of loading cases must be analyzed. In DNVGL-ST-0437 [20] a table is presented detailing several situations that the wind turbine can go through during its lifespan such as power production, production with the occurrence of a control system fault, normal shutdown, emergency stops, etc. Some of these situations, for example, guide the creation of Ultimate Limit State (ULS) or Fatigue Limit State (FLS) loading cases. As the objective of this work is to study the behavior of two different wind turbines by analyzing the sensitivity of fatigue damage, a high number of loading cases was not desired. A smaller selection of cases was made, which allowed to better observe this sensitivity.

The chosen situation in this work was Design Load Case 1.2 (power production). In this situation, Normal Turbulence Model (NTM) is used to represent the wind condition and Normal Sea State model (NSS) is employed for the waves. No current is present in this case.

The obtained Brazilian environmental data, despite revealing important extreme conditions of wave, wind and current, has classes of information not correlated with each other. It is not known the value of the significant wave height (H_S) or its peak period (T_P) for a given mean wind speed. Thus, it is not possible to approximate probability density functions that correlate with each other to form a joint distribution, as strongly recommended by DNVGL-ST-0437 [20]. It was decided to select a few wind speeds in a joint occurrence diagram of intensity and wind direction (Table 9) in association with the SMB (Sverdrup-Munk-Bretschneider) method that is able to obtain the significant wave height and its peak period for a given mean wind speed by knowing the distance *F* over which the wind travels for wave formation (U.S. Army Coastal Engineering Research Center [21]). If the calculated values are shown to be minimally consistent with those present in a scatter diagram of the Brazilian coast's waves (Table 10), the cases may be considered representative of the region. In addition, because of the SMB method, wind and waves were considered aligned although DLC 1.2 indicates the opposite.

To calculate the wave parameters, a hypothetical position was assumed for the wind turbines: 15 kilometers off the Brazilian coast, as shown in the sketch in Fig. 7. Therefore, for a wind coming from the South, the propagation distance is 15 kilometers. For winds coming from the Southwest and Southeast, it is 21.2 kilometers. In the other directions, the winds were considered to be regular for a distance of 150 kilometers. Thus, for the twelve wind speeds chosen (Table 9), and considering these assumptions, we have the values of H_S and T_P (or zero crossing period T_Z) indicated in Table 11.

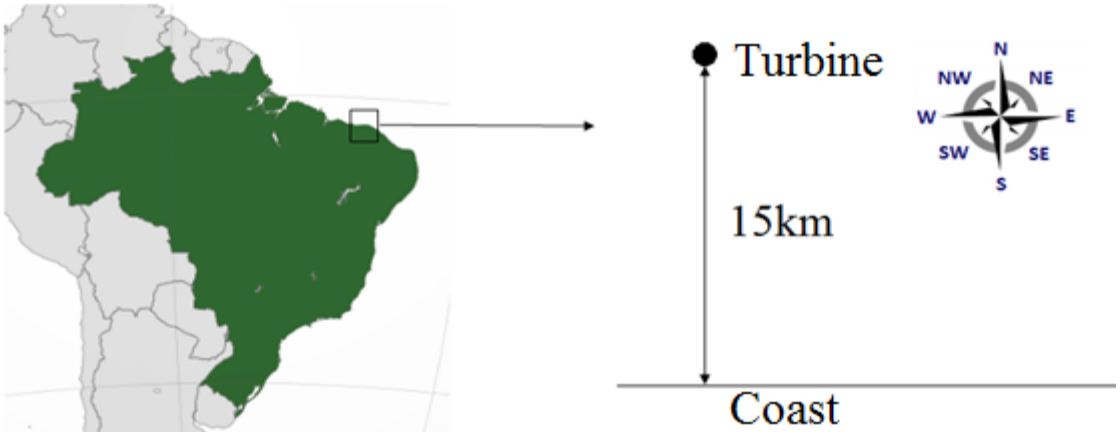

Figure 7. Sketch: Hypothetical position of the wind turbines (adapted from Nogueira [8]).

Table 9 shows the occurrence of each wind speed as a function of direction (where it comes from) and intensity (in m/s). These values come from wind speed measurements at a height of 10 meters above the mean-sea level over an hour. In other words, the intensity represents an average hourly value. The selected values are highlighted in yellow. The criteria for choosing them were the wind speeds being in the wind turbines operating intervals (between cut-in and cut-out) and the highest number of occurrences per direction. The aim was also to vary wind speeds as much as possible.

Table 9 shows that most occurrences come from the East and Southeast and the most common speeds are 7, 8 and 9 m/s. In Table 10, it is observed that the most frequent significant wave height is between 1 - 1.5 meters and the peak period is between 5 - 6 seconds. The highest H_S value found is 2.5 meters and T_P is 23 seconds with only one occurrence.

Table 9. Joint occurrence of intensity and wind direction (true North). (Nogueira [8]).

M/S		DIRECTION (º)								Freq	%	Mean Dir
		N	NE	E	SE	S	SW	W	NW			
0	1	51	50	49	52	44	38	24	24	332	0.41	93.4
1	2	123	134	173	256	86	37	24	60	893	1.11	93.3
2	3	124	270	398	557	133	33	25	54	1594	1.98	101
3	4	68	458	690	1186	177	31	13	32	2655	3.3	107
4	5	56	510	1451	2378	262	20	13	15	4705	5.85	112
5	6	16	552	2647	4169	294	14	3	5	7700	9.57	113
6	7	15	560	4017	5570	271	6	1	1	10441	13	112
7	8	2	373	5064	5877	193	1	0	3	11513	14.3	110
8	9	0	182	5706	5555	186	4	0	0	11633	14.5	109
9	10	0	53	5208	4403	116	0	0	0	9780	12.2	108
10	11	0	15	4598	3177	42	0	0	0	7832	9.74	106
11	12	0	3	3606	2006	11	0	0	0	5626	7	105
12	13	0	3	2370	1177	1	0	0	0	3551	4.42	105
13	14	0	2	1099	517	0	0	0	0	1618	2.01	105
14	15	0	0	320	156	0	0	0	0	476	0.59	106
15	16	0	0	48	22	0	0	0	0	70	0.09	107
16	17	0	0	1	1	0	0	0	0	2	0	112
17	18	0	0	0	0	0	0	0	0	0	0	0
Freq		**455**	**3165**	**37445**	**37059**	**1816**	**184**	**103**	**194**	**80421**		
%		**0.6**	**3.94**	**46.56**	**46.08**	**2.26**	**0.2**	**0.1**	**0.24**			
Mean Int		**2.7**	**5.23**	**8.72**	**7.82**	**5.71**	**2.8**	**2.3**	**2.42**	**8.03**		

Table 10. Significant wave height distribution by peak period (Nogueira [8]).

Hs (m)		Tp (s)																				Freq	%	Mean Tp
		4	5	6	7	8	9	10	11	12	13	14	15	16	17	18	19	20	21	22				
		5	6	7	8	9	10	11	12	13	14	15	16	17	18	19	20	21	22	23				
0.0	0.5	0	0	0	0	0	0	0	0	0	0	0	0	0	0	0	0	0	0	0	**0**	**0.0**	**0.0**
0.5	1.0	73	105	105	101	105	63	34	53	41	37	16	4	0	0	0	0	0	0	0	**737**	**6.9**	**8.3**
1.0	1.5	832	1105	822	763	638	612	306	306	369	392	330	119	55	7	14	1	0	2	1	**6674**	**62.7**	**8.5**
1.5	2.0	378	781	378	222	160	230	165	116	120	179	160	81	75	21	26	6	4	1	0	**3103**	**29.1**	**8.6**
2.0	2.5	3	46	24	5	2	8	23	13	0	1	2	2	5	0	3	0	1	0	0	**138**	**1.3**	**8.6**
2.5	3.0	0	0	0	0	0	0	0	0	0	0	0	0	0	0	0	0	0	0	0	**0**	**0.0**	**0.0**
Freq		**1286**	**2037**	**1329**	**1091**	**905**	**913**	**528**	**488**	**530**	**609**	**508**	**206**	**135**	**28**	**43**	**7**	**5**	**3**	**1**	**10652**		
%		**12.1**	**19.1**	**12.5**	**10.2**	**8.5**	**8.6**	**5.0**	**4.6**	**5.0**	**5.7**	**4.8**	**1.9**	**1.3**	**0.3**	**0.4**	**0.1**	**0.1**	**0.0**	**0.0**			
Mean Hs		**1.4**	**1.4**	**1.4**	**1.3**	**1.3**	**1.3**	**1.4**	**1.4**	**1.3**	**1.4**	**1.4**	**1.5**	**1.6**	**1.6**	**1.6**	**1.8**	**1.9**	**1.5**	**1.4**			

Table 11. Loading cases created and their occurrences (Nogueira [8]).

Case	Direction	U_m (m/s)	F (km)	H_S (m)	T_P (s)	T_Z (s)	Occurrence	P (%)
1	N	5	150	0.7	3.6	2.5	56	0.21
2	NE	7	150	1.2	4.6	3.3	560	2.15
3	E	9	150	1.6	5.4	3.8	5706	21.86
4	E	12	150	2.2	6.3	4.5	3606	13.82
5	E	13	150	2.4	6.6	4.7	2370	9.08
6	SE	8	21.2	0.7	3.4	2.4	5877	22.52
7	SE	10	21.2	0.9	3.7	2.6	4403	16.87
8	SE	11	21.2	1.0	3.9	2.8	3177	12.17
9	S	6	15	0.4	2.7	1.9	294	1.13
10	SW	5	21.2	0.4	2.6	1.8	20	0.08
11	W	5	150	0.7	3.6	2.5	13	0.05
12	NW	5	150	0.7	3.6	2.5	15	0.06

None of the values found in Table 11 exceeded the 2.5 meters H_S limit, which is a good sign for the SMB method. Considering that wind speeds were selected with the highest occurrences in each direction, it was expected to obtain wave characteristics equally present in Table 10. For cases with wind speeds of at least 7 m/s and propagation distance of 150 km, the results obtained were satisfactory and seem to fit the H_S-T_P distribution measured in the Brazilian coast. Low wind speeds and short propagation distances, however, resulted in cases with excessively low H_S and/or T_P. Despite this, it was decided to use all twelve cases in the following analyses.

The wind turbine class IA [22] is typical of offshore regions and it is characterized by the most turbulent properties. It is an expected class for a 10 MW turbine, since more powerful and robust wind turbines are typically deployed in these regions. However, this class was adopted for both turbines in the loading cases to create the most conservative analysis possible.

Table 12 summarizes important parameters that were used in the wind and wave modeling in TurbSim and SIMA-RIFLEX software. It should be noted that the performed analyses on both of them were 3800 seconds long of which the first 200 seconds were discarded. This is because these first seconds represent a transient part of the response (start of rotor operation). Thus, we have a usable time of 3600 seconds in both programs. It is noteworthy that, for each loading case, it was considered the wind acting on the rotor frontally, i.e. the rotation angle of the rotor in all cases was equal to zero.

Table 12. TurbSim and SIMA-RIFLEX inputs (Nogueira [8]).

Rating	5 MW	10 MW
TurbSim's grid points	31 x 31	31 x 31
TurbSim's grid height	132 m	186 m
TurbSim's grid width	132 m	186 m
Simulation length	3800 s (200 s cutoff)	
TurbSim's timestep	0.05 s	
Wind spectrum	Kaimal	
IEC edition used in TurbSim	3rd edition [22]	
IEC Turbulence class	A	
Wind model in TurbSim	NTM	
Mean wind speed profile	Power-law	
Power-law exponent	0.14	
Peakedness parameter for Jonswap Spectrum	3.3	
Hydro force formulation	Morison	
Inertia coefficient	2.0	
Drag coefficient	0.9	
SIMA-RIFLEX's timestep	0.01 s	
S-N Curve adopted	D (seawater with cathodic protection) [5]	

Finally, to study the sensitivity of fatigue damage, four types of analyses were performed as shown in Table 13. Static wind means that the wind was modeled only as an average invariant time profile according to power-law. The dynamic wind employed the same static mean profile accompanied by a dynamic portion generated by the Kaimal spectrum. In each type of analysis, 12 loading cases were evaluated (Table 11). Since there are two distinct wind turbines, a total of 96 analyses were executed.

Table 13. Types of analyses (Nogueira [8]).

Representation	Type 1	Type 2	Type 3	Type 4
Wave	Jonswap	Pierson-Moskowitz	Jonswap	Pierson-Moskowitz
Wind	Static	Static	Dynamic	Dynamic

3.4 Results

For a type 3 analysis, the annual damage of points 1 to 4 of the 5 MW wind turbine's critical cross section is presented in Table 14 without considering the probabilities of occurrence of each loading case, according to Eq. (5). Then, for this scenario, the damage with this probability accounted for, according to Eq. (6), is presented and thus the total damage can be obtained (Table 15). The probabilities of occurrence of each case are derived from Table 9. They are presented again in Table 11 and exclude the other unused occurrences, such that the probability of these 12 loading cases computes 100% of the annual occurrences. This assumption is present in the damage calculations of all analyses, which are available in Appendix A of Nogueira [8]. The greatest damage in each case is highlighted in red.

Table 14. 5 MW – Type 3: Annual damage without occurrence accounting (Nogueira [8]).

Case	Direction	Point 1	Point 2	Point 3	Point 4
1	N	8.23E-04	1.15E-04	9.46E-08	2.02E-04
2	NE	1.19E-03	8.04E-06	1.62E-03	6.76E-03
3	E	5.93E-05	3.24E-03	1.32E-02	2.74E-03
4	E	6.74E-04	8.52E-03	2.29E-02	5.07E-03
5	E	2.06E-03	1.90E-02	3.20E-02	7.08E-03
6	SE	1.21E-03	4.33E-03	8.88E-04	2.40E-05
7	SE	2.52E-03	8.38E-03	1.96E-03	1.24E-04
8	SE	3.81E-03	1.03E-02	2.34E-03	2.38E-04
9	S	1.71E-03	2.47E-04	2.82E-07	4.39E-04
10	SW	9.58E-05	6.54E-08	1.64E-04	6.83E-04
11	W	9.46E-08	2.02E-04	8.23E-04	1.15E-04
12	NW	2.02E-04	8.23E-04	1.15E-04	9.46E-08

Table 15. 5 MW – Type 3: Annual damage accounting for occurrence (Nogueira [8]).

Case	Direction	Point 1	Point 2	Point 3	Point 4
1	N	8.23E-04	1.15E-04	9.46E-08	2.02E-04
2	NE	1.19E-03	8.04E-06	1.62E-03	6.76E-03
3	E	5.93E-05	3.24E-03	1.32E-02	2.74E-03
4	E	6.74E-04	8.52E-03	2.29E-02	5.07E-03
5	E	2.06E-03	1.90E-02	3.20E-02	7.08E-03
6	SE	1.21E-03	4.33E-03	8.88E-04	2.40E-05
7	SE	2.52E-03	8.38E-03	1.96E-03	1.24E-04
8	SE	3.81E-03	1.03E-02	2.34E-03	2.38E-04
9	S	1.71E-03	2.47E-04	2.82E-07	4.39E-04
10	SW	9.58E-05	6.54E-08	1.64E-04	6.83E-04
11	W	9.46E-08	2.02E-04	8.23E-04	1.15E-04
12	NW	2.02E-04	8.23E-04	1.15E-04	9.46E-08
Total Damage		1.50E-03	7.25E-03	9.81E-03	2.15E-03

This pattern of results shown in Tables 14 and 15 repeats itself in all other analyses (Table 13) presented in Nogueira [8]. It is observed that for environmental loads coming from North and South, points 1 and 5 suffered the most damage. For Northeast and Southwest, the points were 4 and 8. For East and West, the points were 3 and 7 and, finally, for Northwest and Southeast, points 2 and 6 showed the greatest fatigue damage. Figures 8 and 9 justify this phenomenon, taking as an example, case 3 (East) analyzed in model 3 (5 MW offshore) under the conditions generated by a type 3 analysis (dynamic wind and Jonswap spectrum).

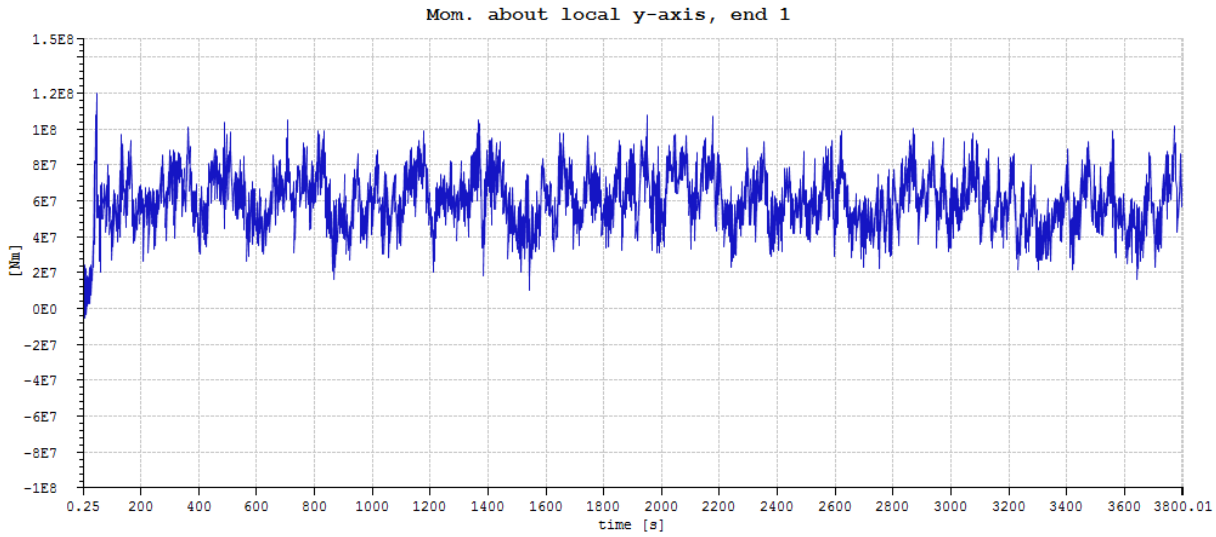

Figure 8. Model 3, Type 3, Case 3 (East): Moment about local Y-axis (Nogueira [8]).

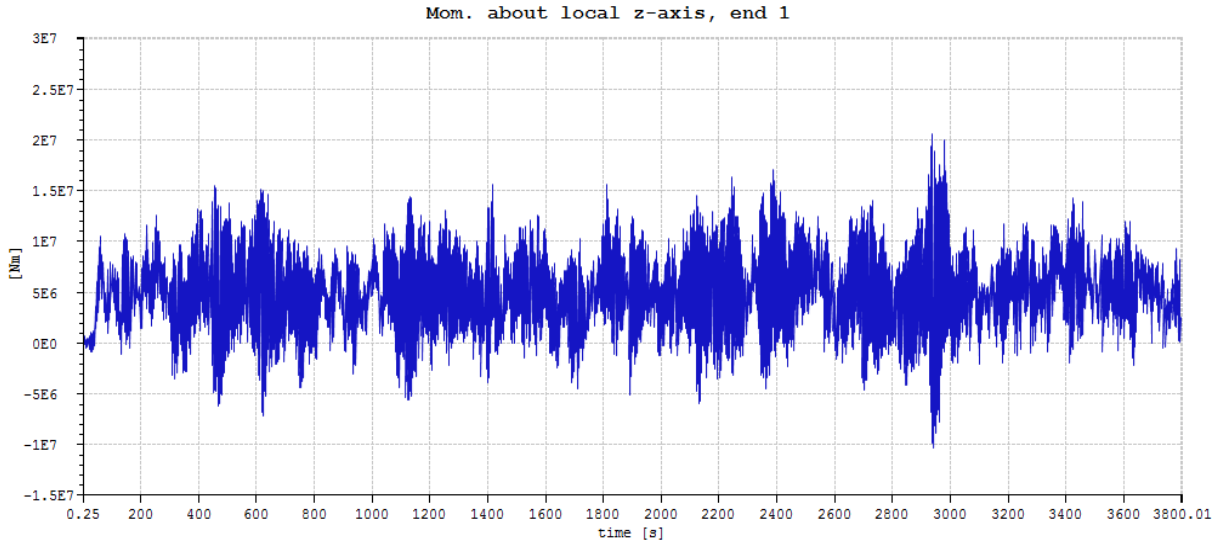

Figure 9. Model 3, Type 3, Case 3 (East): Moment about local Z-axis (Nogueira [8]).

Note that the maximum moments in Fig. 8 are about 5 times greater than the maximum values in Fig. 9. Analyzing both figures, it is observed that the moment variation in the Y direction is about 3 times greater than in the Z direction. As a result, the damage caused at the cross-section points that are aligned with the direction of the environmental loads (in this case, 3 and 7 according to Fig. 4) is considerably greater.

Figures 10 and 11 show the same behavior described for Fig. 8 and 9, but referring to the 10 MW model (model 4). It is observed that the moment values, in absolute numbers, are not much higher than those presented in Fig. 8 and 9. Consequently, when transforming these bending moments into stress, lower values are obtained for model 4, which justifies the structure's lifespan presented in Table 16.

In addition, looking at Table 15, it is concluded that the greatest damage was caused by loading cases 3, 4, and 5 (from the East). These cases are characterized by wind speeds close to the nominal speed (higher thrust force) and by the highest values of H_S and T_P/T_z, due to the longer propagation distances (150 kilometers). Cases 6, 7 and 8 also caused considerable damage to the 10 MW turbine (Nogueira [8]). Despite the lower H_S, the waves' peak periods are closer to the first natural frequencies of model 4 (resonance), which justifies these results.

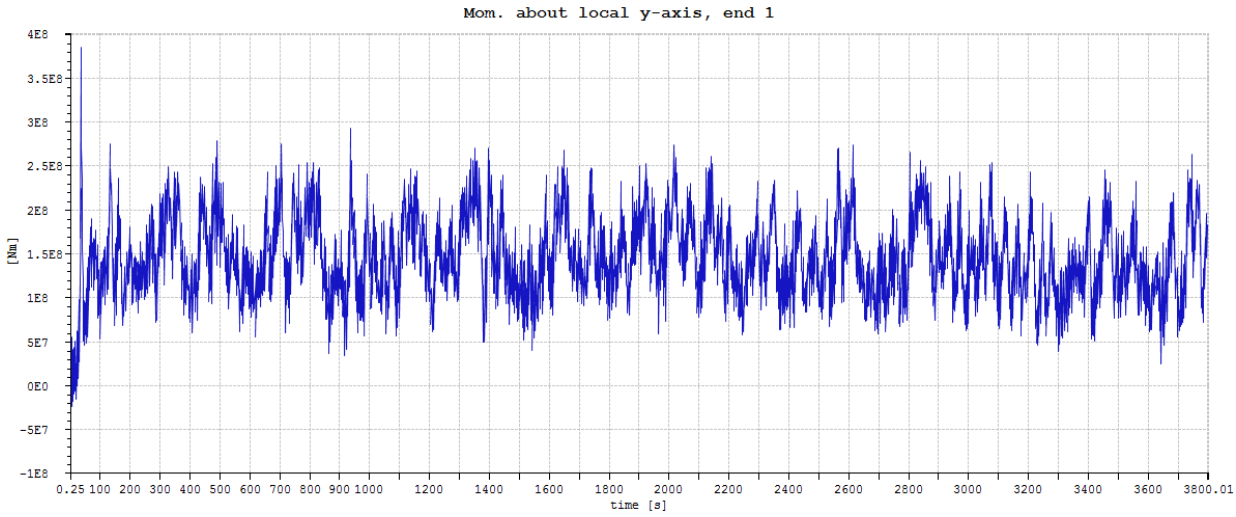

Figure 10. Model 4, Type 3, Case 3 (East): Moment about local Y-axis (Nogueira [8]).

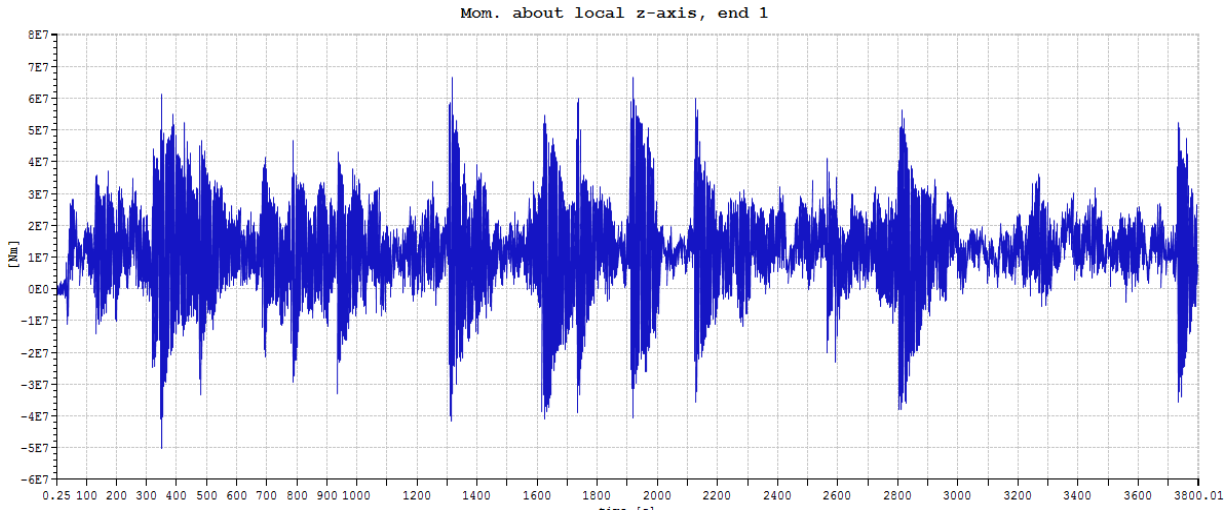

Figure 11. Model 4, Type 3, Case 3 (East): Moment about local Z-axis (Nogueira [8]).

Table 16. Lifespan summary (Nogueira [8]).

Turbine	Type	Point 1	Point 2	Point 3	Point 4
5 MW	1	213000	9530	1890	8670
	2	162000	7470	1550	7240
	3	666	138	102	465
	4	609	143	108	443
10 MW	1	916000	78200	22400	111000
	2	766000	67000	18000	86700
	3	4860	969	679	2980
	4	4430	896	629	2810

Looking at Table 16 some comments can be made:

1. Type 3 and 4 analyses, which consider wind with its dynamic portion, had a much shorter life when compared to Types 1 and 2, where only static wind is present. Failure to consider wind turbulence increases foundation lifespan by at least one order of magnitude;

2. Looking at the lifespan obtained for Type 3 and 4 analyses of the same turbine, it can be concluded that when the wind is realistically represented, the wave spectrum used is not a major factor. The differences obtained for the same turbine, in this situation, were around 5 to 10%;
3. As the lifespan of a wind turbine is around 20 years, the foundation of both turbines can be considered suitable for this simplified FLS, given the shortest lives obtained (102 and 629 years respectively).

4 Conclusions

In this work, a sensitivity analysis of fatigue damage in the foundation of two distinct wind turbines was performed. For this, models 3 and 4, defined in item 2.1, had a critical cross section of their respective foundations analyzed, as described in Table 13. Based on the information and results presented in this paper, the following observations and conclusions are made:

1. The critical point of both monopiles are in the distance range of once the foundation's diameter (4.5 meters and 7.5 meters, according to item 3.2) below the mudline;
2. For environmental loads coming from North and South, points 1 and 5 suffered the most damage. For Northeast and Southwest, the points were 4 and 8. For East and West, the points were 3 and 7. Finally, for Northwest and Southeast, points 2 and 6 showed the most damage;
3. Type 3 and 4 analyses, which consider wind with its dynamic portion, showed much higher damage when compared to Types 1 and 2, where there is only static wind. This consideration is very important since disregarding wind turbulence increases foundation lifespan by at least an order of magnitude;
4. Looking at the lifespan obtained for Type 3 and 4 analyses of the same turbine, it can be concluded that when the wind is realistically represented, the wave spectrum used is not a major factor. The differences obtained for the same turbine, in this situation, were around 5 to 10%.
5. As the lifespan of a wind turbine is around 20 years, the foundation of both turbines can be considered suitable for this simplified FLS, given the shortest lives obtained (102 and 629 years respectively).
6. The greatest damage was caused by loading cases 3, 4 and 5 from the East. These cases are characterized by wind speeds close to the nominal speed and by the highest values of H_S and T_P/T_Z due to the greater propagation distances (150 kilometers).
7. Cases 6, 7 and 8 also caused considerable damage to the 10 MW turbine (Nogueira [8]). Despite the lower H_S, the waves' peak periods are closer to the first natural frequencies of model 4 (resonance), which justifies these results
8. Evaluating Table 16, it can be noted that the 5 MW wind turbine had a shorter lifespan than the 10 MW in all analyses. This is due to the higher stiffness of the 10MW turbine, which promoted lower stress variations.

Acknowledgements

The study described in this paper is the result of a partnership between Petrobras and UFRJ and was carried out with resources from the R&D program of the Electricity Sector regulated by ANEEL, under the PD-00553-0045/2016 project titled "Planta Piloto de Geração Eólica Offshore".

The authors would also like to express their gratitude to "Fundação Carlos Chagas Filho de Amparo à Pesquisa do Estado do Rio de Janeiro" (FAPERJ), "Conselho Nacional de Desenvolvimento Científico e Tecnológico" (CNPq) and "Coordenação de Aperfeiçoamento de Pessoal de Nível Superior" (CAPES), for the resources destined to the production of this research.

References

[1] Ministério de Minas e Energia. Resenha Energética Brasileira 2018 – Ano Base 2017.
[2] J. Jonkman, *et al*. Definition of a 5-MW Reference Wind Turbine for Offshore System Development. National Renewable Energy Laboratory – NREL, Colorado, USA, 2009.
[3] C. Bak, *et al*. DTU Wind Energy Report-I-0092: Description of the DTU 10 MW Reference Wind Turbine. Copenhagen, Denmark, 2013.
[4] Sintef Ocean. RIFLEX 4.10.3 Theory Manual. 2017.
[5] Det Norske Veritas. Fatigue Design of Offshore Steel Structures: DNV-RP-C203. Norway, 2011.
[6] J. Jonkman and W. Musial. Offshore Code Comparison Collaboration (OC3) for IEA Task 23 Offshore Wind Technology and Deployment. National Renewable Energy Laboratory – NREL, Colorado, USA, 2010.
[7] J. Velarde and E. Bachynski. Design of Monopile Foundations to Support the DTU 10 MW Offshore Wind Turbine. Master thesis, Norwegian University of Science and Technology, Trondheim, Norway, 2016.
[8] G. Nogueira. "Avaliação do comportamento de turbinas eólicas offshore fixas do tipo monopile". Master thesis, Federal University of Rio de Janeiro, RJ, Brazil, 2019.
[9] API. Recommended Practice for Planning, Designing and Constructing Fixed Offshore Platforms – Working Stress Design (RP 2A-WSD). American Petroleum Institute, 21th ed., USA, 2000.
[10] Det Norske Veritas. Design of Offshore Wind Turbine Structures: DNV-OS-J101. Norway, 2014.
[11] B. J. Jonkman and L. Kilcher. Turbsim user's guide: version 1.06.00. Draft version. National Renewable Energy Laboratory – NREL, Colorado, USA, 2012.
[12] P. Maiolino. "Análise dinâmica de turbina eólica offshore do tipo monocoluna". Master thesis, Federal University of Rio de Janeiro, RJ, Brazil, 2014.
[13] M. O. L. Hansen. Aerodynamics of wind turbines. 2nd ed., Earthscan, 2008.
[14] J. Morison *et al*. The Force Exerted by Surfaces Waves on Piles. Petrol. Trans., AIME, nº 189, 1950.
[15] T. Sarpkaya and M. Isaacson. Mechanics of Wave Forces on Offshore Structures. Van Nostrand Reinhold Company. New York, USA, 1981.
[16] S. K. Chakrabarti. Handbook of offshore engineering. Elsevier. Illinois, USA, 2005.
[17] M. Matsuiski and T. Endo. Fatigue of Metals Subject to Varying Stress. Japan Society of Mechanical Engineers. Fukuoka, Japan, 1968.
[18] J. S. M. Giraldo. Efficient methods for probabilistic fatigue analysis of marine structures. Master thesis, Federal University of Rio de Janeiro, RJ, Brazil, 2014.
[19] A. Bøhn. Fatigue Loads on Large Diameter Offshore Wind Monopile Foundations in Non-operational Situations. Master thesis, Norwegian University of Science and Technology, Trondheim, Norway, 2016.
[20] Det Norske Veritas - Germanischer Lloyd. Loads and site conditions for wind turbines: DNVGL-ST-0437. Norway, 2016.
[21] U.S. Army Coastal Engineering Research Center. Shore Protection Manual, vol. 1. Vicksburg, Mississippi, USA, 1984.
[22] International Electrotechnical Commission. IEC 61400-1: Wind turbines – Part 1: Design requirements. 3rd ed., 2005.